Chapter-6

Bi and Gd Co-Substituted Cubic Zirconia Based Oxide-ion Conductor

6.1 Introduction

In ZrO_2-based materials, a combination of high dielectric permittivity and thermal stability with low leakage current due to a reasonably high barrier height that limits electron tunnelling counts it to further research as an oxide-ion conductor for SOFCs application.[1-3]

Yttria stabilized zirconia (YSZ) is considered the most effective candidate as a solid electrolyte for electrochemical cells working either in open-circuit mode (oxygen sensor) or in a power application (oxygen pump and SOFCs) due to its robustness.[1-7] . Y_2O_3 stabilized ZrO_2 (YSZ) material was first recognized by Nernst in 1890s as a potential electrolyte owing to their high oxide-ion conductivity. Among the various Y_2O_3-ZrO_2 solid solutions, 8 mol% Y_2O_3-ZrO_2 is reported to exhibit highest ionic conductivity of 0.1 S/cm at 1000^oC.[8] Further continuous research was going on to increase the oxide-ion conductivity of YSZ. Studies have shown that doping trivalent ions (rare earth metals) are more effective than divalent ions (alkali metals), mainly because of the higher defect association tendency and the lower thermodynamic stability of cubic fluorite. For trivalent ions, the doping effect on oxygen ion conductivity is mainly in the order of Eu < Gd < Dy < Y < Er < Yb < Sc. Among them, Sc_2O_3 stabilized ZrO2 (ScSZ) demonstrated the highest ionic conductivity, reaching as great as 0.003 S cm^{-1} at 500 °C.[9-11] However, very high cost and scarcity of scandium made ScSz as a non-viable oxide-ion electrolyte for SOFCs.

Since the discovery of superior oxide-ion conductivity in Mg-doped perovskite structure $Na_{0.5}Bi_{0.5}TiO_3$[12]; a well-known piezoelectric material that possesses high leakage conductivity that makes the material unsuitable for piezo- and ferroelectric applications, newer interest is open to developing superior oxide-ion conducting materials through controlling the nature of dielectricity of the materials. The fast oxygen ion diffusion of $Na_{0.5}Bi_{0.5}TiO_3$ (NBT) is attributed to the high polarizability of Bi^{3+} and is mediated by oxygen vacancies[1] that can be introduced either by changing the NBT compositions through

Bi deficiency or by Mg doping[12-13] dielectric leakage or relaxor-like characteristics of ferroelectrics or high k dielectric materials reveal as a substantial temperature and frequency dependence in the maximum of both real and imaginary part of dielectric permittivity. However, relaxors not only show particular and intriguing behaviours in the dielectric response, also show promising activity in fast-ion conduction to be applied as an oxide-ion conductor for the application in solid oxide fuel cells (SOFCs), oxygen separation membranes, oxygen sensors and oxygen pumps.[14-20] Also, Bi-based oxide-ion conductors demonstrate remarkable ionic conductivity due to high-concentration intrinsic oxygen vacancies and high polarizability of Bi^{3+} with $6s^2$ lone pair electrons.[4]

This chapter demonstrates that relaxor nature of high k dielectricity and higher polarizability of Bi^{3+} ion seems to play a directive role in providing superior oxide-ion transport throughout the lattice at a temperature close to dielectric relaxation temperatures.[12,15,27] ZrO_6 octahedra was a feudal point in developing superior-high κ dielectric/ferroelectric materials, especially in PZT based perovskite structures. The relaxor nature of high dielectric constant materials is also reported for doped cubic Zirconia phases.[21-24] We have envisaged that high polarizability of Bi^{3+} ion couple with high k dielectric relaxation (high dielectric leakage) can generate superior oxide-ion conduction near T_m (The temperature of the maximum *dielectric permittivity*). To realize the concept, we attempted the suitable doping of Bi^{3+} and Gd^{3+} ions into the ZrO_2 lattice to stabilize the cubic phase. Here, we present the synthesis, characterization, permittivity and oxide-ion conductivity studies of Bi^{3+} and Gd^{3+} substituted cubic zirconia in this chapter.

6.2 Material's synthesis

$Zr_{1-x-y}Bi_xGd_yO_{2-\delta}$ samples were synthesized by employing the solution combustion method by dissolving a stoichiometric amount of ZrO $(NO_3).xH_2O$, Bi_2O_3 and Gd_2O_3 in 100 ml of 40% nitric acid solution with continuous stirring at 90° C for 4-5 hours. Further, for auto-combustion, glycine was used as the fuel and was added in a molar ratio of 1.5:1 to the total moles of cation present in the solution. The temperature of the hot plate-magnetic stirrer was increased to 250°C for combustion to start. Reaction ends up with vigorous combustion after the evaporation of water at gelation point due to constant heating. The material left behind after combustion was collected, and multiple calcinations were carried out at 900°C for 12 hours to get single-phase materials. For conductivity measurement, the powder was made into pellets of 10 mm diameter and ~0.2-0.25cm thickness by pressing it to 7-8 ton weight on a hydraulic press. These pellets were fired at 1000°C for 10 hours for densification. The density of the pellet was measured using the Archimedes method. It was found to be ~97% of the apparent density obtained from the geometrical analysis.

6.3 Material's Characterization

The phase formation study was carried out through Rigaku Miniflex desktop X-ray Diffractometer (XRD) with Cu-Kα radiation (λ = 1.54 Å) in the range 2θ ~ 10 - 90° with a step size of 0.02°. The structures were refined by the Rietveld refinement method using the FULLPROF suite software package and cubic fluorite ZrO_2 (space group: Fm3m) as model structure. The microstructures of the sintered samples were investigated by using scanning electron microscopy (EVO - Scanning Electron Microscope MA15/18). The average grain size was calculated using the linear intercept method. The composition of the compounds was examined by Energy dispersive X-ray (EDX) spectroscopy with a probe attached to the SEM instrument. Raman spectroscopy of powdered sample was carried out by using STR-300

micro-Raman spectrometer with a laser excitation wavelength of 532 nm and step size of $1.9\ cm^{-1}$.

Pt paste was used as a current collector for conductivity measurements. For this purpose, the sintered pellets were coated with platinum paste and cured at 800°C for 30 minutes. The conductivity measurements were performed using Autolab potentiostat as a function of frequency from 1 MHz to 1 Hz at different temperatures varying from 100°C to 650°C. All measurements were taken during the cooling cycle from 650°C to 100° C.

6.4 Crystal Structure Analysis

As Gd^{3+} ions can stabilized the ZrO_2 in cubic fluorite structure[2], the role or promoting effect of Bi^{3+} ion were utilized to develop superior oxide-ion conductors. Several compositions of $Zr_{1-x-y}Gd_xBi_yO_{2-\delta}$ in cubic fluorite structure were synthesized, and a few important data were presented in this chapter. We have found that at max, 40% ions can be substituted at Zr site to make single-phase cubic fluorite material using Gd^{3+} and Bi^{3+} as a simultaneous substituents. Thus, Up to 20% of Bi and 30% of Gd were co-substituted in the ZrO_2 lattice ($Zr_{1-x-y}Gd_xBi_yO_{2-\delta}$, $x+y\leq 0.4$, $x \leq 0.3$ and $y \leq 0.2$) in different combinations and several solid solutions were synthesized in cubic fluorite structure. The synthesized Bi^{3+} and Gd^{3+} substituted ZrO_2 powder was off-white in colour. The crystal structure and phase purity of the material was analyzed by powder XRD study. Powder XRD pattern of $Zr_{0.6}Bi_{0.2}Gd_{0.2}O_{2-\delta}$ (B20G20), $Zr_{0.6}Bi_{0.15}Gd_{0.25}O_{2-\delta}$ (B15G25), $Zr_{0.65}Bi_{0.15}Gd_{0.20}O_{2-\delta}$ (B15G20), $Zr_{0.7}Bi_{0.15}Gd_{0.15}O_{2-\delta}$ (B15G15), and $Zr_{0.6}Bi_{0.10}Gd_{0.30}O_{2-\delta}$ (B10G30), are shown Figure 6.1(a-e) respectively. All the peaks were identified to cubic fluorite yttria-stabilized zirconia (YSZ) structure (JCPDS No: 98-001-9128). No impurity peaks were identified for Gd_2O_3, Bi_2O_3 or any other phases of pure ZrO_2. Thus single-phase materials were synthesized using a solution combustion route with multiple calcinations at 900^oC for 12 hours. Crystal structures of Bi

and Gd substituted ZrO_2 were refined using the Rietveld method. Figure 6.2 shows the representative Rietveld refined XRD profile for (a) $Zr_{0.6}Bi_{0.2}Gd_{0.2}O_{1.8}$ and (b) $Zr_{0.6}Bi_{0.1}Gd_{0.3}O_{1.8}$. The fitted profile matched well with the observed XRD pattern. The structural parameters obtained from Reitveld refinement of powder XRD pattern are given in Table 6.1. Due to the substitution of larger Bi^{3+} and Gd^{3+} cations on the Zr site in the ZrO_2 lattice, there was an increase in the lattice parameter of the materials with an increase in the concentration of dopants.

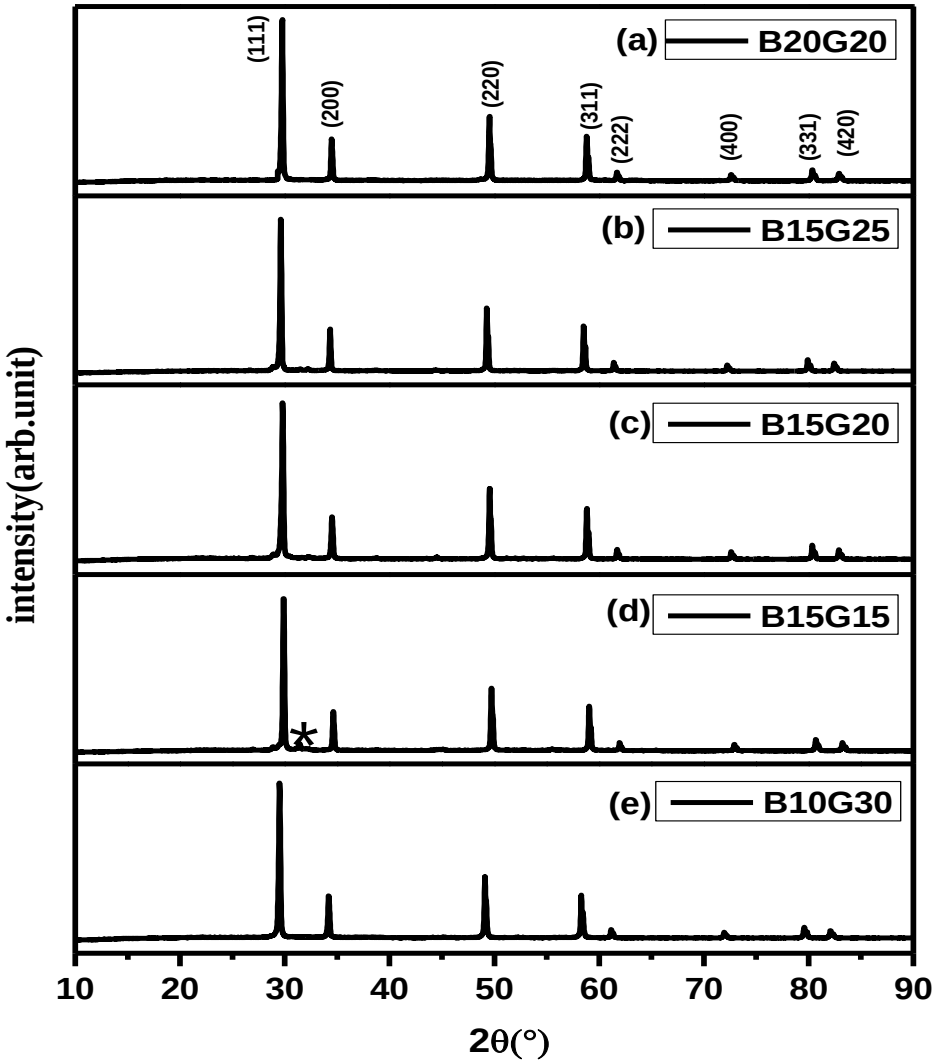

Figure 6.1 Powder XRD pattern (i)$Zr_{0.6}Bi_{0.2}Gd_{0.2}O_{1.8}$, (ii)$Zr_{0.6}Bi_{0.15}Gd_{0.25}O_{1.8}$, (iii)$Zr_{0.65}Bi_{0.15}Gd_{0.2}O_{1.825}$, (iv)$Zr_{0.7}Bi_{0.15}Gd_{0.15}O_{1.85}$, and (v)$Zr_{0.6}Bi_{0.10}Gd_{0.30}O_{1.8}$

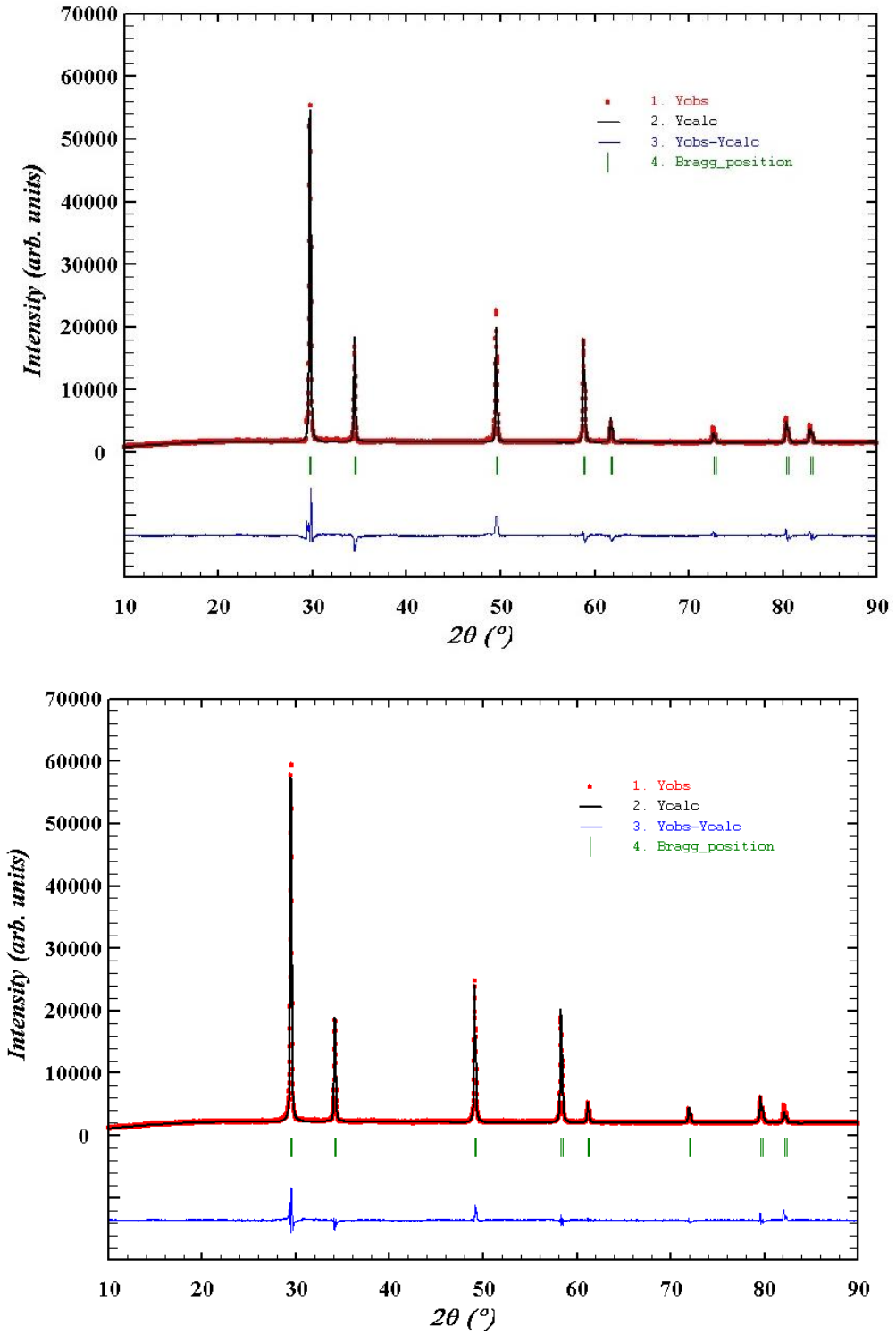

Figure 6.2. Rietveld refined powder XRD profile of (i)$Zr_{0.6}Bi_{0.2}Gd_{0.2}O_{1.8}$,

(ii)$Zr_{0.6}Bi_{0.10}Gd_{0.30}O_{1.8}$

Table 6.1: Structural parameter of Bi and Gd doped ZrO_2

Compound	**Lattice parameter(Å) (a=b=c)**	χ^2	R_f	R_{Bragg}
ZrO_2	*5.13 (Ref. 19)*	-	-	-
$Zr_{0.6}Bi_{0.2}Gd_{0.2}O_{1.8}$	5.2444(2)	2.86	3.51	5.18
$Zr_{0.6}Bi_{0.15}Gd_{0.25}O_{1.8}$	5.2362(1)	3.07	6.96	7.49
$Zr_{0.65}Bi_{0.15}Gd_{0.2}O_{1.825}$	5.2298(3)	3.43	6.29	8.71
$Zr_{0.7}Bi_{0.15}Gd_{0.15}O_{1.85}$	5.2392(2)	6.12	7.23	9.54
$Zr_{0.6}Bi_{0.10}Gd_{0.30}O_{1.8}$	5.2021(3)	6.94	9.54	12.41

6.5 SEM/EDAX Study

SEM micrographs of $Zr_{0.6}Bi_{0.2}Gd_{0.2}O_{1.8}$ (powder, top view and cross-section of the pellet used for conductivity measurements) are shown in Figure 6.3 (a-c). The SEM study shows that the powders are made of interconnected grains of 4–10 μm. Figures 6.3 (b and c) show the pellet's top and cross-section images. Crystal growth during sintering resulted in microstructure having nearly no or very low porosity, and the grains are thoroughly interconnected (good contact with each other). Further, no colour contrasts were observed in the SEM images representing the uniform distribution of elements in the grains of the materials. The EDX study (micrograph shown in Figure 6.3d) also confirms that the composition of the materials is similar to the nominal composition taken for the synthesis.

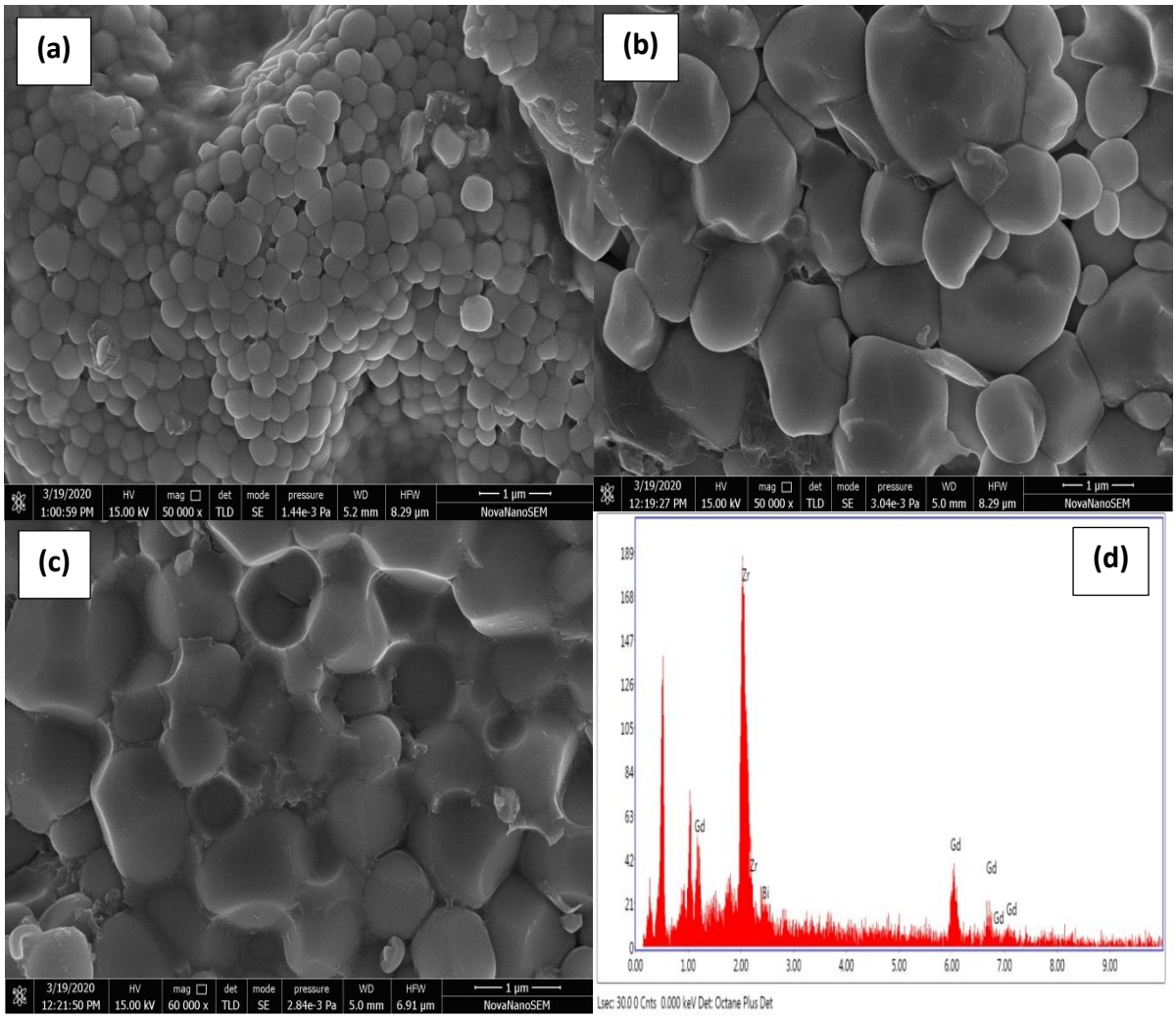

Figure 6.3. SEM image $Zr_{0.6}Bi_{0.2}Gd_{0.2}O_{1.8}$ (a) Powder (b) Front view of the pellet (c) Cross-section of the pellets and (d) EDX image of pallet

Thus XRD, SEM coupled with EDX study confirms that Bi^{3+} and Gd^{3+} ions are substituted at Zr^{4+} sites in stabilized cubic ZrO_2 lattice. Considering the intrinsic stiometric defects formation due to the substitution of Bi^{3+} and Gd^{3+} at Zr^{4+} sites that will create oxygen vacancy generation in the lattice and the oxygen defect formation equation using Kröger–Vink notation can be represented as:

$$Bi_{Zr}^{'} + Gd_{Zr}^{'} \leftrightarrow V_o^{\cdot\cdot} \qquad \text{eq.(6.1).}$$

Further, the lone pair of Bi^{3+} ions can stabilize the oxide-ion vacant fluorite structure, as represented in Figure 6.4. The lone pair of Bi^{3+} ion is known to implant higher vacancy mobility, as was witnessed in the case of Bi-based oxide-ion conductors.[1, 4, 21-26]

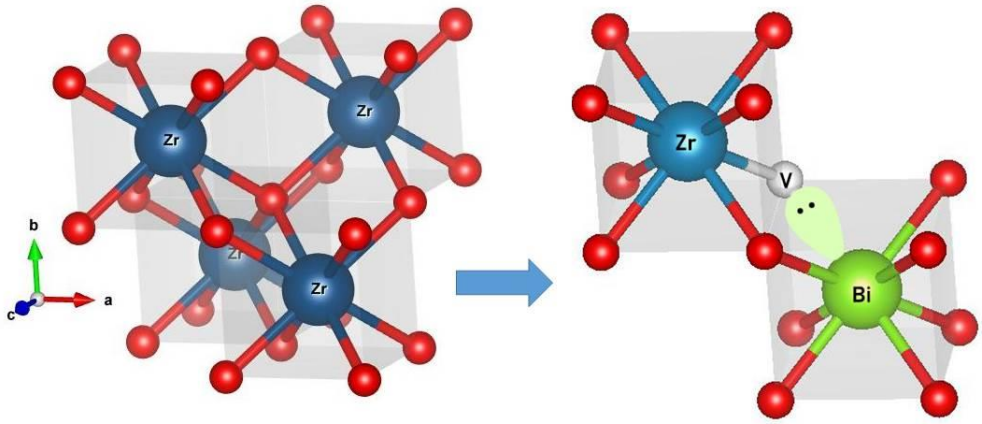

Figure 6.4 Vacancy mapping through Bi lone pair in cubic fluorite structure.

6.6 Raman Spectroscopy Analysis

Figure 6.5 presents the Raman spectra of (a) undoped monoclinic Zirconia and (b) Gd/Bi co-doped cubic Zirconia ($Zr_{0.6}Bi_{0.2}Gd_{0.2}O_{1.8}$). The Raman spectrum for cubic ZrO_2 is characterized by a narrow band at 145 cm^{-1} and broad bands centered around 250, 305, 440, and ~601 cm^{-1}. The stabilized ZrO_2 sample in this study clearly showed the broad peak between 500 to 650 cm^{-1} that is related to the disordered oxygen sub-lattice along with mass-related disorder, indicating a significant disorder in the cationic cage upon Gd and Bi ion substitution in cubic ZrO_2 lattice. In contrast, monoclinic ZrO_2 exhibits several well defined sharp bands because of the symmetry reduction.[33] Since the cations are much heavier than the oxygen atoms; they are the major contributors to the vibrations associated with the acoustic branches indicating a periodic arrangement of the vacancies in stabilized Gd/Bi co-doped cubic- zirconia the lattice.[34-36] A careful examination of the Raman spectra also show weak bands around 620, 660, and 815 cm^{-1} that could be associated with the rearrangement of the

anionic sub-lattice, i.e. oxygen ions and vacancies containing Bi cage in stabilized Bi/Gd co-doped cubic zirconia.[37] Further observed bands around 535 nm and 790 nm can be assigned to Raman vibrations of Gd containing sublattice of stabilized Bi/Gd co-doped cubic zirconia.[38] Thus, the Raman spectroscopy study clearly reveal the formation of oxygen vacant Gd/Bi co-doped cubic Zirconia lattice.

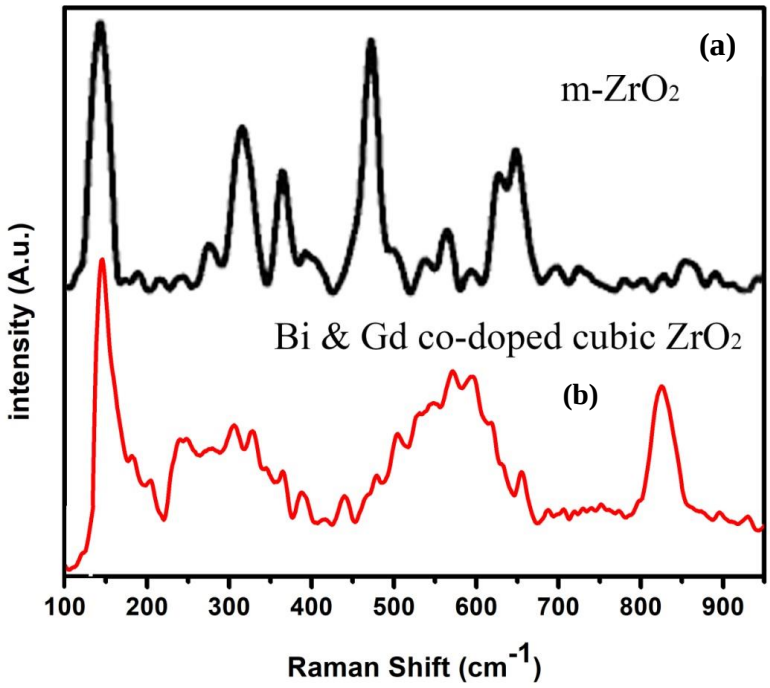

Figure 6.5 Raman spectra of (a) monoclinic ZrO_2 and (b) Gd-Bi co-doped cubic Zriconia ($Zr_{0.6}Bi_{0.2}Gd_{0.2}O_{1.8}$).

6.7 Impedance Study

To see the effect of Gd and Bi substitution in fluorite ZrO_2 structure, impedance spectroscopy was utilized to study the oxide-ion vacancy conduction process and dielectric constant of the materials at various temperatures in different environments. Figure 6.6 show the conductivity plot for different composition of Bi and Gd substituted ZrO_2 i.e. (i) $Zr_{0.6}Bi_{0.2}Gd_{0.2}O_{1.8}$ (B20G20), (ii) $Zr_{0.6}Bi_{0.15}Gd_{0.25}O_{1.8}$ (B15G25), (iii) $Zr_{0.65}Bi_{0.15}Gd_{0.2}O_{1.825}$ (B15G20), (iv) $Zr_{0.7}Bi_{0.15}Gd_{0.15}O_{1.85}$ (B15G15), and (v) $Zr_{0.6}Bi_{0.10}Gd_{0.30}O_{1.8}$ (B10G30). The

total electrical conductivity was found continuously increase with increasing temperature for all the compositions. The best electrical conductivity of this series was observed for the composition $Zr_{0.6}Bi_{0.2}Gd_{0.2}O_{1.8}$. At 550°C, the measured conductivity was ~10^{-2} S.cm^{-1} for $Zr_{0.6}Bi_{0.2}Gd_{0.2}O_{1.8}$, which is better than that of $Zr_{0.92}Y_{0.08}O_2$ (YSZ) at 670°C at and of $La_{0.8}Sr_{0.2}Ga_{0.83}Mg_{0.17}O_3$ (LSGM) at 600°C. The Data for oxide-ion conductivity of different samples of $Zr_{1-x-y}Bi_xGd_yO_{2-(x+y)/2}$ at different temperatures, along with the data of another competitive oxide-ion electrolyte in the same temperature range, is given in Table 6.2.

Table 6.2: O^{2-} conductivity (σ) of $Zr_{1-x-y}Bi_xGd_yO_{2-\delta}$ at different temperatures

	Conductivity (S.cm^{-1})			
Compound	***650°C***	**600°C**	**550°C**	**500°C**
$Zr_{0.85}Gd_{0.15}O_{1.925}$	1.0x10^{-2}	3.5x10^{-3}	1.2x10^{-3}	3.2x10^{-4}
$Zr_{0.80}Gd_{0.20}O_{1.9}$	1.4x10^{-2}	4.4x10^{-3}	1.9x10^{-3}	4.3x10^{-4}
$Zr_{0.75}Gd_{0.25}O_{1.875}$	1.1x10^{-2}	4.9x10^{-3}	1.6x10^{-3}	4.8x10^{-4}
$Zr_{0.70}Gd_{0.30}O_{1.85}$	1.0x10^{-3}	3.8x10^{-3}	2.1x10^{-3}	2.2x10^{-4}
$Zr_{0.6}Bi_{0.2}Gd_{0.2}O_{1.8}$	6.2x10^{-2}	3.2x10^{-2}	1.1x10^{-2}	1.9x10^{-3}
$Zr_{0.6}Bi_{0.15}Gd_{0.25}O_{1.8}$	2.6x10^{-2}	1.6x10^{-2}	7.9x10^{-3}	3.6x10^{-4}
$Zr_{0.65}Bi_{0.15}Gd_{0.2}O_{1.825}$	1.8x10^{-2}	8.8x10^{-3}	2.8x10^{-3}	2.7x10^{-4}
$Zr_{0.6}Bi_{0.15}Gd_{0.15}O_{1.85}$	1.6x10^{-2}	1.2x10^{-2}	2.3x10^{-3}	1.2x10^{-4}
$Zr_{0.7}Bi_{0.10}Gd_{0.30}O_{1.8}$	1.2x10^{-2}	4.8x10^{-3}	1.8x10^{-3}	4.2x10^{-4}
$KTa_{0.4}Ti_{0.3}Ge_{0.3}O_{2.7}$ (Ref. 37)	5.2x10^{-2}	3.1x10^{-2}	9.8x10^{-3}	8.5x10^{-3}
$Na_{0.5}Bi_{0.49}Ti_{0.98}Mg_{0.02}O_{2.965}$ (Ref. 29)		6.6x10^{-3}	5.4x10^{-3}	3.5x10^{-3}
$Zr_{0.92}Y_{0.08}O_{1.96}$ (Ref. 29)		4.4x10^{-3}	2.3x10^{-3}	1x10^{-3}
$Ce_{0.9}Gd_{0.1}O_{1.95}$ (Ref. 29)		2.3x10^{-2}	1.2x10^{-2}	6.5x10^{-3}
$La_{0.9}Sr_{0.1}Ga_{0.9}Mg_{0.1}O_{2.9}$ (Ref. 29)		2.5x10^{-2}	1.5x10^{-2}	6.5x10^{-3}

Impedance study of $Zr_{0.6}Bi_{0.2}Gd_{0.2}O_{1.8}$ was also carried out at different temperatures in dry hydrogen (UHP H_2) and dry nitrogen (UHP N_2) environments (Figure 6.7) also to see the effect of the absorbed moisture, and impurities present in the air on the surface or at oxide-ion vacancy sites of the sample and also the stability of the material in reducing environment in the presence of hydrogen. Below 500°C, the total conductivity of $Zr_{0.6}Bi_{0.2}Gd_{0.2}O_{1.8}$ was found to be a little lower in the Hydrogen and Nitrogen atmosphere compared to air. In the cubic fluorite phase of ZrO_2, YSZ is predominantly a total oxide-ion conductor. Below 500°C, Gd and Bi-doped ZrO_2 sample in air atmosphere may have little bit associate protonic conduction contribution due to presence of existing moist into the air. Moisture present in the air can result in the absorption of moisture on the sample's surface at low temperatures contributing to additional conductivity at those temperatures. As we have not found any increase in total conductivity in hydrogen atmosphere even at higher temperatures, this suggests the stability of Bi^{3+} ion in ZrO_2 lattice that does not allow the reduction Bi^{3+} ions in hydrogen media. The cole-cole plot at 500°C in the air atmosphere for $Zr_{0.6}Bi_{0.2}Gd_{0.2}O_{1.8}$ is shown for understanding the polarization and oxide-ion transport nature of the sample (Figure 6.8). The linear tail present in the plot suggests ionic conduction pathways. Thus the total conductivity in Gd and Bi codoped ZrO_2 sample is ionic and facilitates oxide-ion conductivity due to oxygen vacancy migration. Further, we have also characterized the $Zr_{0.6}Bi_{0.2}Gd_{0.2}O_{1.8}$ sample heated in 10% hydrogen balanced in nitrogen atmosphere at 800°C for 6h by powder XRD study and we have not found any diffraction peaks for Bi metal in the XRD of the sample as all the peaks were identified to cubic phase of Zirconia only (Figure 6.10). Further no colour changes were observed for the sample heated in H_2 atmosphere at 800°C for 6h. These studies clearly suggest the material's stability in reducing media and suggest that the total conductivity of our samples are predominantly an oxide-ion conduction as Gd^{3+} and Bi^{3+} doped sample contain oxide-ion vacancy. A

comparison of oxide-ion conductivity of $Zr_{0.6}Bi_{0.2}Gd_{0.2}O_{1.8}$ in the same temperature range of 300–650°C with other established oxide-ion conductors having crystal structures of Fluorite or Perovskite also presented in (Figure 6.9). Oxide-ion conductivity of $Zr_{0.6}Bi_{0.2}Gd_{0.2}O_{1.8}$ (ZBGO) is very much comparable to Sr and Ga doped $LaGaO_3$; LSGM and $KTa_{0.4}Ti_{0.3}Ge0.3O_{2.7}$(KTTGO). The activation energy for oxide-ion conductivity was found to be as low as 0.42 eV. In the case of all samples, a sudden increase in oxide-ion conductivity was found at or around 450^{o}C.

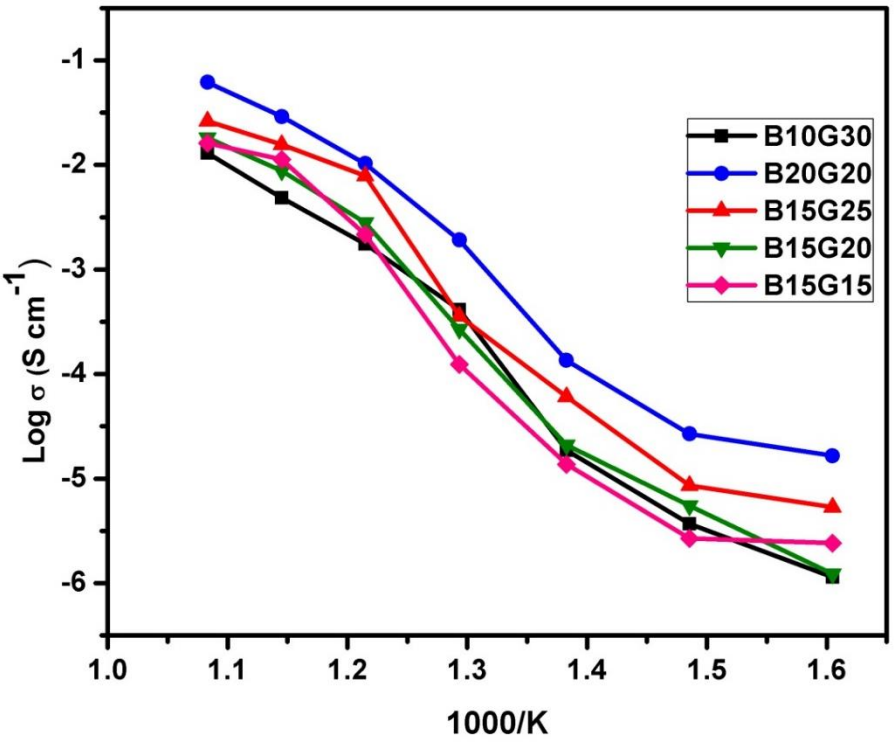

Figure 6.6. Arrhenius plot of various compositions

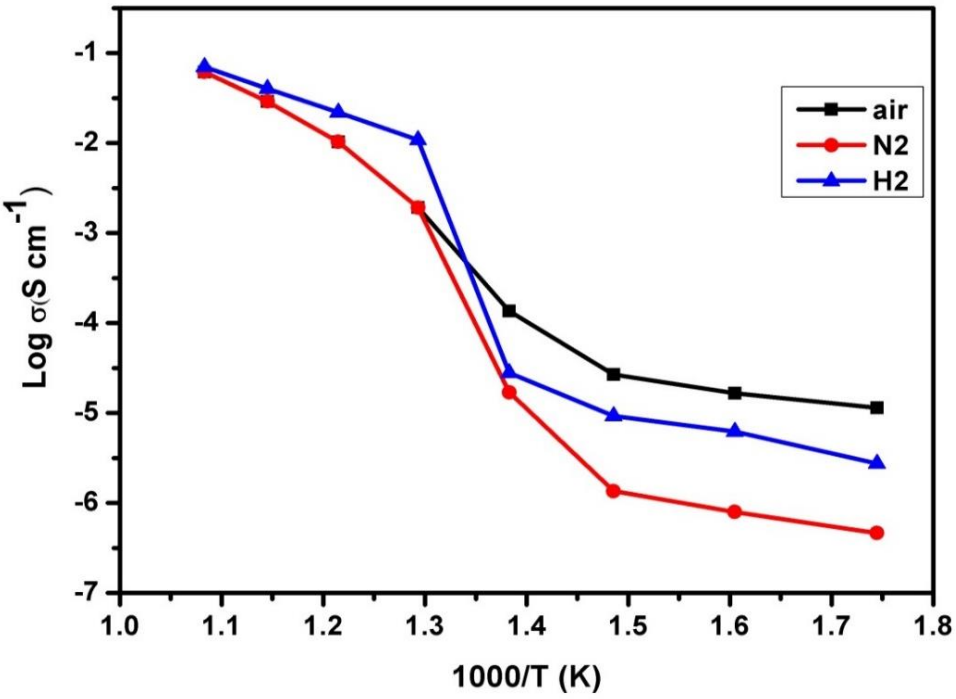

Figure 6.7 . Arrhenius plot of $Zr_{0.6}Bi_{0.2}Gd_{0.2}O_{1.8}$ (ZBGO) in different medium

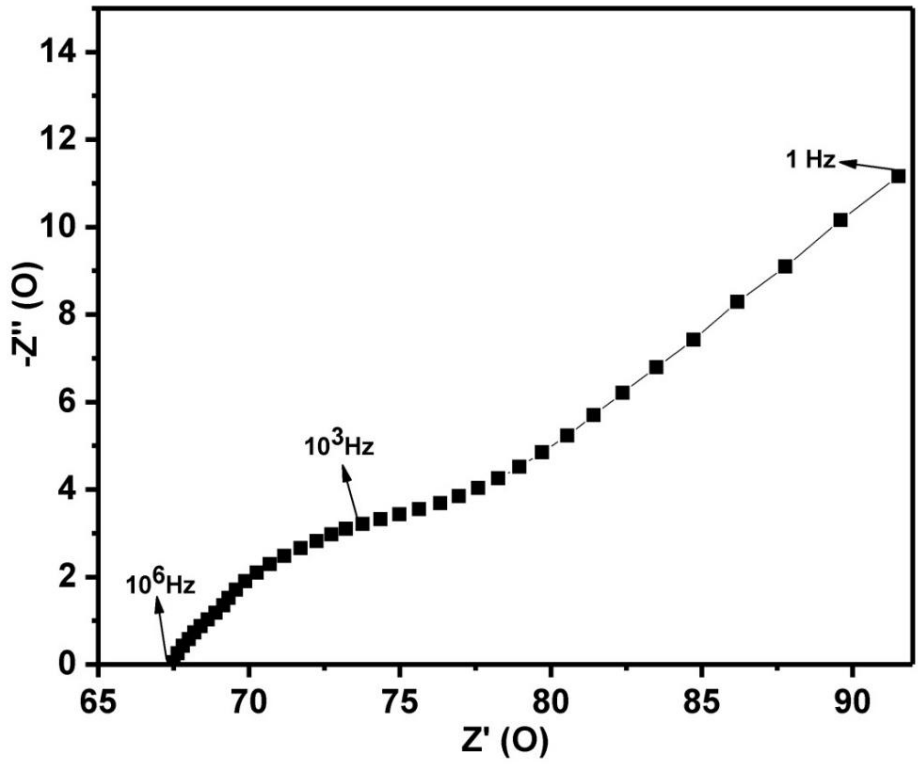

Figure 6.8. Cole-Cole plot of $Zr_{0.6}Bi_{0.2}Gd_{0.2}O_{1.8}$ at 500 ^{o}C

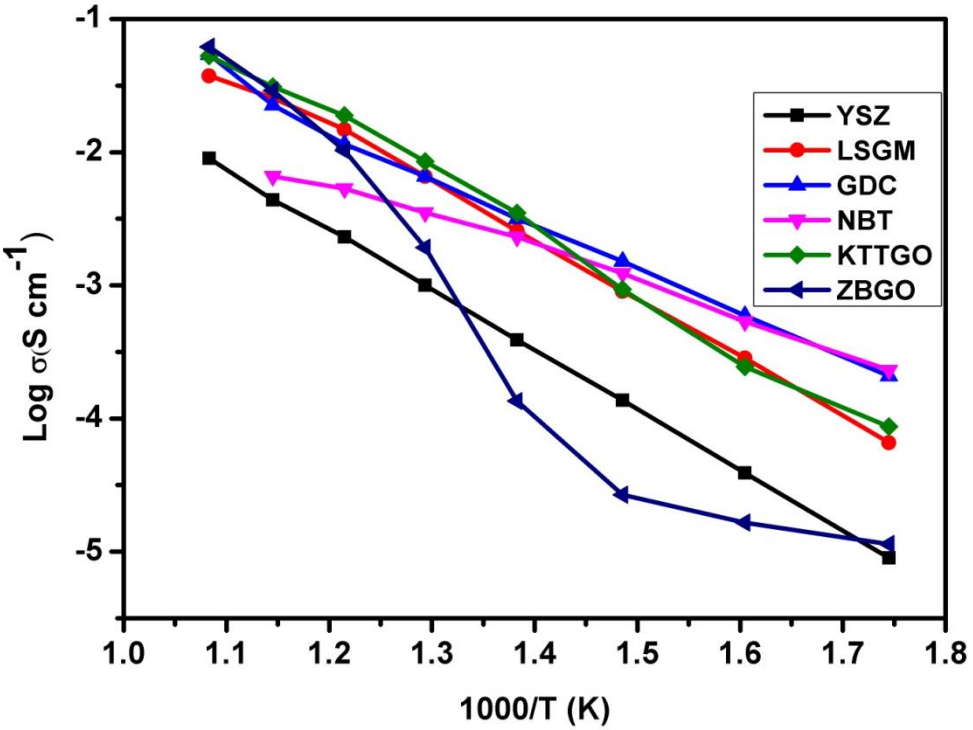

Figure 6.9. Arrhenius plot of comparison of existing intermediate temperature Oxide-ion electrolytes in air (data taken from Ref.1)

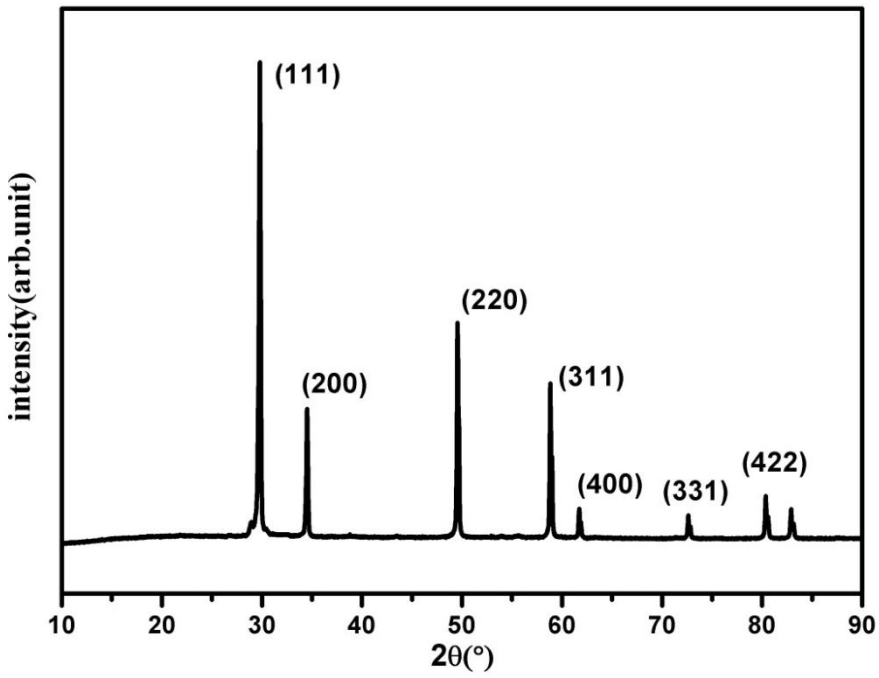

Figure 6.10 Powder XRD pattern of $Zr_{0.6}Bi_{0.2}Gd_{0.2}O_{1.8}$ heated in hydrogen atmosphere up 800^{o}C during impedance study.

6.8 Thermal Study

Further to understand the sudden increase in conductivity if it is associated with any phase transformation, Thermogravimetric and Differential Scanning Calorimetry (TGA-DSC) analysis at a constant heating rate of 10^oC/minute in the temperature range of 30^oC - 900^oC in N_2 atmosphere. Fig. 6.11 shows the TGA plot for $Zr_{0.6}Bi_{0.2}Gd_{0.2}O_{1.8}$ sample preheated at 120^oC. The lack of physically adsorbed water on the sample was demonstrated as marginal weight loss was observed up to 150^oC followed by very little weight loss (~0.5%) up to 900^oC. The TGA analysis confirms the relatively low hygroscopicity or dry nature of the material. The DSC curve shown in Figure 6.11 does not show any significant feature for any associated phase change that may arrive from oxide-ion vacancy or structure reorientation. Thus the TGA/DSC studies confirm the structure stability of the material in the temperature range of 30^oC-900^oC. In addition, an FT-IR study was also performed to monitor the presence of hydroxide-ions or water absorption at the oxygen vacancy position or at the surface of the Bi and Gd co-substituted ZrO_2 samples. Figure 6.12 displays the FT-IR spectra of $Zr_{0.6}Bi_{0.2}Gd_{0.2}O_{1.8}$ sample preheated at 120^oC for about 1 hour. Absence of peaks between 3300-4000 cm^{-1} clearly suggests the absence or insignificant presence of hydroxide-ions or physio-adsorbed water on the surface of the material. This confirms that the conductivity observed for cubic fluorite $Zr_{1-x-y}Bi_xGd_yO_{2-(x+y)/2}$ samples are only due migration of oxide-ion vacancies in the lattice.

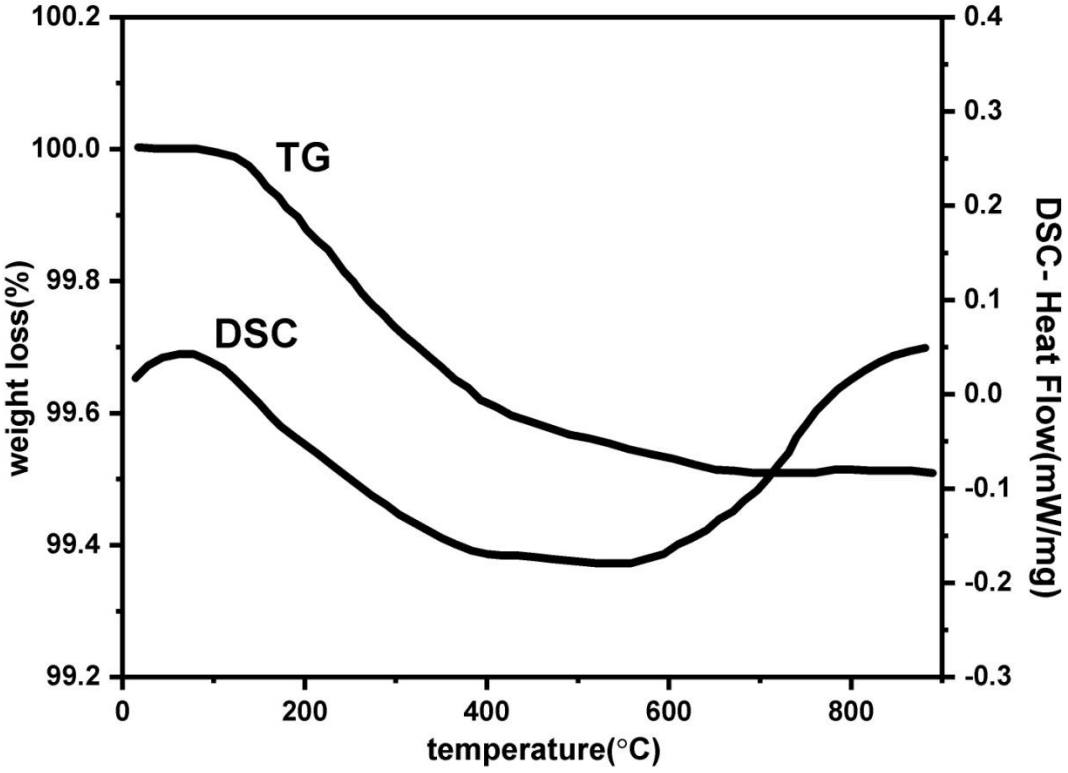

Figure 6.11. TGA and DSC curves of $Zr_{0.6}Bi_{0.2}Gd_{0.2}O_{1.8}$ preheated at 120°C

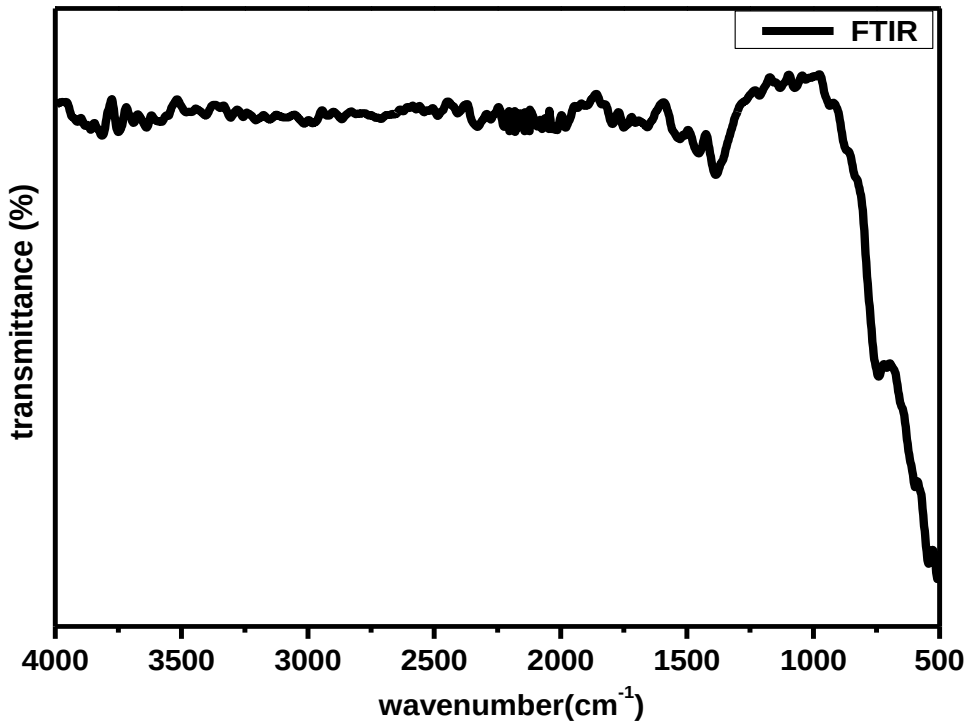

Figure 6.12. FT-IR spectra of $Zr_{0.6}Bi_{0.2}Gd_{0.2}O_{1.8}$ preheated at 120°C

The sudden change or activation of oxygen vacancy migration above 450^{o}C confirms the oxide-ion transport within the percolation limit of a conductive phase transition coupled with thermal activation. Further to understand the effect of dielectric polarizability on oxide-ion conductivity, the dielectric constant in the frequency range of 20 kHz to 100 KHz at different temperatures is plotted in Figure 6.13. The dielectric studies show a relaxor type behavior coupled with diffusive phase transition characterized by the permittivity dependence on the temperature and on applied frequencies. $Zr_{0.6}Bi_{0.2}Gd_{0.2}O_{1.8}$ sample show a significant ε_{max}' (maximum permittivity) equivalent to ~9725 at 600^{o}C at applied frequency 20 kHz, much higher than those for the pure ZrO_2. With increasing applied frequency, the T_m had varied and observed to decrease. This gradual decrease with increasing applied frequency confirms the relaxor behaviour of this high κ dielectric material. Also, these compositions show a rather high dielectric loss (tan δ > 100) above ~400°C, that increases exponentially with temperature above 600°C (Figure 6.14) suggesting high leakage current at elevated temperatures. The dielectric relaxation of the dipole moment can lead to the material's superior oxide-ion conductivity at the temperature close to T_m. The relaxation of net dipole moment generated over oxygen vacant octahedra can play a vital role in reorientation of the polyhedra at elevated temperature to provide the short transport pathways for the oxide-ion vacancy migration. Thus this giant loss (high leakage) seems to be associated with conduction or migration of oxide vacancy.

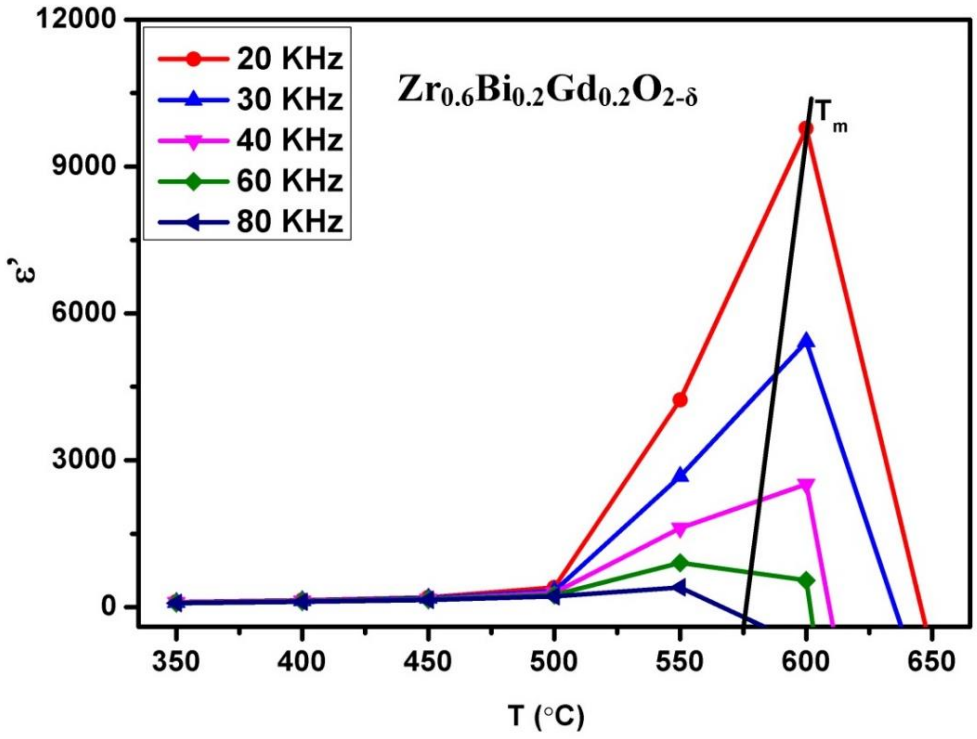

Figure 6.13. Dielectric constant of $Zr_{0.6}Bi_{0.2}Gd_{0.2}O_{1.8}$ at different temperatures and frequencies

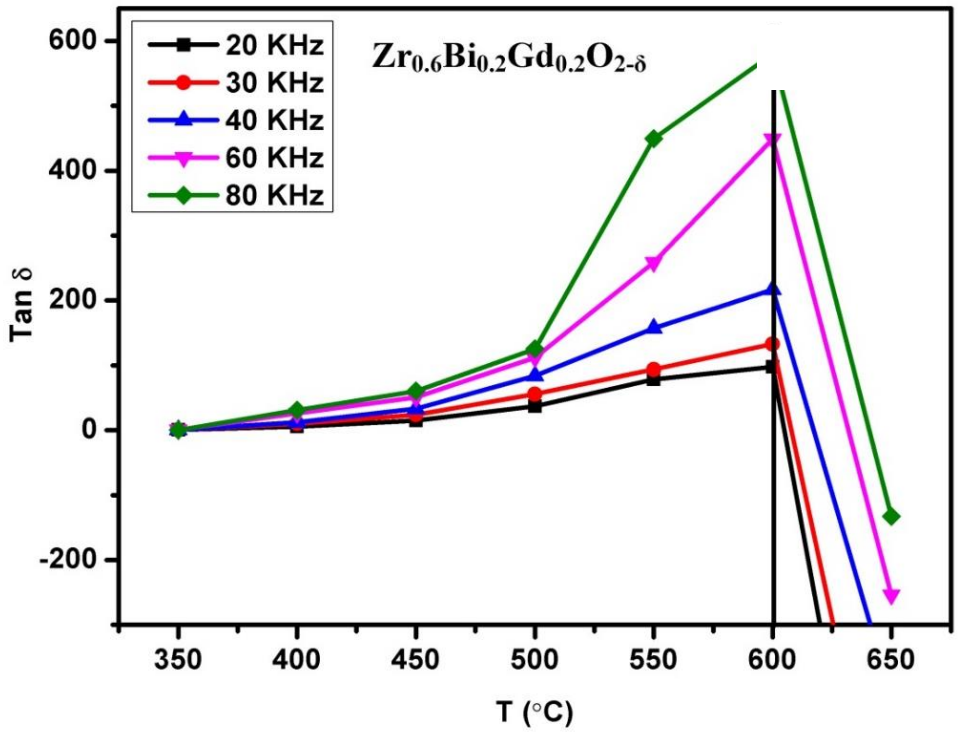

Figure 6.14. Dielectric loss of $Zr_{0.6}Bi_{0.2}Gd_{0.2}O_{1.8}$ at different temperatures and frequencies.

It is well known that higher concentration of oxide-ion vacancies at lattice sites and their high mobility are two key factors for achieving high ionic conductivity in typical oxide-ion conductors. For cubic zirconium oxides, oxide-ionic conduction is primarily associated with the conducting passageway through a cubic block and the movement of oxygen vacancies dominates. Similar to PZT-based ferroelectric ceramics, the vibration of a smaller-sized Ti^{4+} and Ge^{4+} cation from its mean position in octahedral coordination was shown to have the high dielectric constant and relaxor type behaviour and associated high oxide-ion conductivity in $KTa_{0.4}Ti_{0.3}Ge_{0.3}O_{2.7}$.[16] Here, Bi^{3+} and Gd^{3+} ions doped into ZrO_2 lattice to stabilize the materials in cubic phase and the lone pair of Bi^{3+} ions can also play a vital role in enhancing the polarizability of the solid solution. Further, the synergistic interaction by introducing a secondary substituent (Gd^{3+} ions) seem to play important role to enhance the oxide-ion vacancy transport within the percolation limit ion transport inside the host structure at lower temperatures. High polarizability of Bi^{3+} with $6s^2$ lone pair electrons has been viewed as a key factor for high ionic conductivity in Bi-based oxide conductors, *e.g.*, δ-Bi_2O_3[36], $Bi_4Ti_3O_{12}$[16], γ-$Bi_4V_2O_{11}$[39]. Similarly, in the present material, the $6s^2$ lone pairs of Bi^{3+} ions can be oppositely pointed toward a vacant central of the Zr plane and ZrO_8 polyhedra in the parent-phase as shown in figure 6.6. Also, this structure can have a relaxed unit cell with longer Zr–O bonds, where the oxygen vacancy can jump by thermal activation to the energetically equivalent neighbouring oxygen sites of the lattice cell. However, more advanced structural and phase transition studies such as neutron powder diffraction (NPD) or EXAFS studies at various temperatures are important for the making mechanistic propositions about the associated phase transition responsible for sudden increase in conductivity of the materials at elevated temperatures. However, the direct correlation of dielectric relaxation of dipole moments to superior oxide-ion transport was also observed previously for $Na_{0.5}Bi_{0.5}TiO_3$[12-14], $KTa_{1-x-y}Ti_xGe_yO_{3-\delta}$[16], 20% Sm doped

$CeO_2(Ce_{0.8}Sm_{0.2}O_{2-\delta})$[17] and $La_2Mo_2O_9$[18] . However further studies are necessary to validate the relationship of dielectric relaxation and associated phase transitions that provide shorter conduction pathways for material's superior oxide-ion conductivity.

6.9 Conclusions

In cubic ZrO_2, the theoretical ratio of the ionic radius of the cation to anion (O^{2-}) for a fully packed FCC lattice is 0.73 at room temperature, but the ratio is 0.59 for the tetragonal phase of ZrO_2 stabilized at room temperature.[25] Hence, doping of other elements with a larger ionic radius than Zr at Zr site is an efficient way to stabilize the high-temperature cubic phase at room temperature by the formation of solid solutions. Our study shows that the co-doping of Bi^{3+} and Gd^{3+} ions (ionic radii in 8 coordinations, Bi^{3+} = 1.17 Å and Gd^{3+} = 1.053Å)[20] in ZrO_2 lattice resulted in the formation of Zr-Bi-Gd-O solid solution in cubic phase at room temperature. Also, it resulted in superior oxide-ion transport (oxide-ion conductivity ~10^{-2} S/cm above 500^{o}C) at lower temperatures. The material also showed the relaxor type dielectric nature of solid solution coupled with synergistic interaction of Gd and Bi in solid solution $Zr_{1-x-y}Bi_xGd_yO_{2-\delta}$. a careful study was made on development to superior ZrO_2 based electrolyte. As Gd can stabilized the ZrO_2 in cubic fluorite structure, role or promoting effect of Bi^{3+} ion were utilized to develop superior oxide-ion conductors. We have found that at max, total 40% ions can be substituted at Zr site to make single phase cubic fluorite material. Systematically, we carried out ionic conductivity study of Gd stabilized ZrO_2 for 15%, 20%, 25%, 30% Gd^{3+} ions doping in ZrO_2 and ionic conductivity data of these materials are provided in table 6.2. It was found that 20 and 25% Gd stabilized cubic ZrO_2 showed almost similar conductivities. Further to improve the conductivity of Gd stabilized cubic ZrO_2, Gd^{3+} and Bi^{3+}ion co-substituted cubic Zirconia was synthesized.. In first attempt additional 15% Bi^{3+} co-doping was attempted along with Gd^{3+} ions. However, in case of 30% Gd stabilized

Zirconia, only 10% additional Bi^{3+} can be doped in single phase. Among them, we $Zr_{0.65}Gd_{0.20}Bi_{0.15}O_{2-\delta}$ showed highest conductivity. Further we extended Bi^{3+} ion substitution in Gd stabilized cubic Zirconia and found that highest conductivity can be achieved with $Zr_{0.6}Gd_{0.2}Bi_{0.2}O_{2-\delta}$ sample. Thus this study can confirm that maximum 40% substitution in ZrO_2 lattice was achieved using Gd^{3+} and Bi^{3+} ions, and the highest conductivity was achieved for cubic fluorite $Zr_{0.6}Gd_{0.2}Bi_{0.2}O_{2-\delta}$ sample. $Zr_{0.6}Bi_{0.2}Gd_{0.2}O_{1.8}$ sample showed superior oxide-ion conductivity with the lower activation energy in the temperature range of 300-650°C. The oxide-ion conductivity of $Zr_{0.6}Bi_{0.2}Gd_{0.2}O_{1.8}$ was found 10^{-2} s/cm at or above 500°C. Considering the robustness of ZrO_2 based systems, the materials can act as an possible candidates as an oxide-ion electrolyte for lntermediate temperature solid oxide fuel cells (IT-SOFCs), as the material requires low processing cost and delivers high conductivity at relatively lower temperatures. Nonetheless, more studies are required to determine the applicability of the materials as an oxide-ion electrolyte for the production of IT-SOFCs. The cubic $Zr_{1-x-y}Bi_xGd_yO_{2-\delta}$ phase also showed relaxor type high κ dielectric behaviour (έ = 9725 at 600°C at applied frequency 20 kHz for $Zr_{0.6}Bi_{0.2}Gd_{0.2}O_{1.8}$) with T_m approaching to 600°C. The polarizability of Bi^{3+} ion coupled with high k dielectric relaxation (high dielectric leakage) can utilize as new tool to develop superior oxide-ion conduction near T_m (The temperature of the maximum *dielectric permittivity*) and effort can be made to bring down the T_m to achieve higher ionic conductivity at lower temperatures.